Effect of Zr additions on microstructure evolution and phase formation of Nb−Si based ultrahigh temperature alloys

M. Sankar[a,b,*], G. Phanikumar[b], Vajinder Singh[a], V.V. Satya Prasad[a]

[a] Defence Metallurgical Research Laboratory, Kanchanbagh, Hyderabad 500058, India
[b] Department of Metallurgical and Materials Engineering, Indian Institute of Technology Madras, Chennai 600036, India

A B S T R A C T

In the present work, the role of Zr addition on the microstructure and phase formation of hypoeutectic Nb−16 at. % Si alloy has been investigated. The results showed that both binary and alloy with 2 at. % Zr resulted in two phase microstructures composed of Nb_{ss} and Nb_3Si phases. In contrast, the alloys with 4 at. % Zr and 6 at. % Zr revealed two phase microstructures composed of Nb_{ss} and $\alpha-Nb_5Si_3$ phases. The orientation relationship (OR) obtained between eutectoid lamellar structure comprising of Nb_{ss} and $\alpha-Nb_5Si_3$ phases is (110) Nb//(110) Nb_5Si_3. The equilibrium microstructures consisting of Nb and $\alpha-Nb_5Si_3$ phases were obtained in as cast condition when the Zr concentration is above 2 at.%. The addition of Zr accelerated the dissociation kinetics of Nb_3Si phase in to Nbss and $\alpha-Nb_5Si_3$ phases during solidification. The formation of $\alpha-Nb_5Si_3$ phase in the as cast condition eliminates heat treatment required for decomposition of Nb_3Si phase in Nb-Si alloys.

1. Introduction

Niobium silicide based alloys have been identified as the next generation gas turbine blade materials where the operating temperature is much higher ($> 1150 \, ^{\circ}$C) than the currently used single crystal nickel based superalloys. The high melting temperature ($> 1750 \, ^{\circ}$C), relatively low density (6.6–7.2 g/cc), high temperature strength and good creep resistance make these alloys very attractive for gas turbine applications [1–3]. However, fracture toughness at low room temperature and poor high temperature oxidation resistance limit the use of these alloys. Niobium silicide based alloys are basically in−situ composites developed from binary Nb−Si alloy system consisting of ductile niobium silicon solid solution (Nb_{ss}) and high strength niobium silicides ($Nb_3Si/\alpha-Nb_5Si_3$). The niobium solid solution phase provides room temperature fracture toughness while silicide phase provides high temperature strength and creep resistance. However, it has been reported that the high temperature phase Nb_3Si is retained at room temperature in most of the Nb−Si alloys produced by melting route which is not desirable from high temperature application point of view as it has poor creep properties [4,5]. Further, the Nb_3Si phase undergoes an eutectoid transformation at high temperature to yield Nbss and $\alpha-Nb_5Si_3$ phases. However, the transformation has been reported to be sluggish in nature [6–8].

According to binary Nb−Si phase diagram, the silicide phase Nb_5Si_3 has two allotropic forms. It is body centered tetragonal, $\alpha-Nb_5Si_3$ with $D8_l$ structure (prototype: Cr_5B_3) at low temperature with lattice parameter of a = 0.657 nm and c = 1.1884 nm, and the body centered tetragonal, $\beta-Nb_5Si_3$ with $D8_m$ structure (prototype: W_5Si_3) at high temperature with lattice parameter of a = 1.0018 nm and c = 0.5072 nm [9]. However, the hexagonal $\gamma-Nb_5Si_3$ phase with $D8_8$ structure (prototype: Mn_5Si_3) with lattice parameter of a = 0.752 nm and c = 0.523 nm has also been reported in some of the ternary and multicomponent niobium silicide based alloys [10,11]. Among the all three forms of Nb_5Si_3, the enthalpy of formation of $\alpha-Nb_5Si_3$ phase is more negative (- 64.6 k J mole^{-1}) and the enthalpy of formation of $\gamma-Nb_5Si_3$ phase is less negative (-54.7 k J mole^{-1}). Therefore, the stability of $\alpha-Nb_5Si_3$ phase is much higher than that of other two forms of Nb_5Si_3. Further, both the $\beta-Nb_5Si_3$ and $\gamma-Nb_5Si_3$ phases could be transformed into the stable $\alpha-Nb_5Si_3$ phase after high temperature heat treatment [12–14].

The potential applications of niobium silicide based alloys at very high temperature require a balanced combination of high temperature strength, oxidation resistance and at good fracture toughness at room temperature. Alloying is an effective way of improving these properties by controlling the microstructure during solidification as well as during its subsequent heat treatment processes. Many elements have been added to binary, ternary and multicomponent niobium silicide based alloys in order to improve their properties. It has been reported that the

addition of Ti and Hf resulted in improvement in both room temperature fracture toughness and oxidation resistance [15–18]. However, larger addition of Ti and Hf to Nb−Si alloys has been reported to be stabilize the Nb_3Si phase at lower temperatures as the Nb_3Si, Ti_3Si and Hf_3Si phases form isomorphous system, resulting in the formation of a continuous series of solid solution. Moreover, the melting point of Ti_3Si and Hf_3Si is much lower than that of Nb_3Si [19,20]. The addition of Mo up to 5 at% has been reported to enhance the room temperature fracture toughness. However, the addition of Mo above 5 at % resulted in a decrease of the fracture toughness and oxidation resistance [21]. Kashyap et al. [22] have studied the effect of Ga on near eutectic Nb−Si alloy and found that Ga addition suppresses the formation of Nb_3Si phase and promotes $β−Nb_5Si_3$ phase directly from liquid during solidification. The suppression of Nb_3Si phase and formation of $β−Nb_5Si_3$ phase during solidification has also been reported by Paira et al. [23].

Miura et al. [24] investigated the effect of minor addition of Zr (1.5 at. % Zr) on eutectoid decomposition behaviour of Nb−25 at. % Si alloy and reported that the kinetics of eutectoid transformation of Nb_3Si got accelerated with the addition of Zr. It has also been reported that Zr addition has brought down the time required for the completion of eutectoid transformation of Nb_3Si phase during heat treatment. Tian et al. [25] have studied the effect of Zr additions on microstructure and mechanical properties of ternary alloy Nb−16 at. % Si−22 at. %Ti in the as cast condition and reported that the alloy exhibited three phase microstructure consisting of Nb, Nb_3Si and $γ−Nb_5Si_3$. From the limited number of studies in open literature on the effect of Zr on Nb-Si alloys, it appears that a systematic study on the role of Zr in improving the properties of Nb-Si alloys can lead to promising applications. It has been reported that Nb−Si alloys containing 16–20 at. % Si exhibited superior creep properties [26]. Nb−16 at. % Si belongs to hypoeutectic family of alloys with the presence of Nbss as proeutectic phase. Nbss phase being ductile imparts better toughness compared to alloys containing higher Si content. Hence, in the present study the effect of Zr additions on the microstructure and phase formation of hypoeutectic Nb−16 at. % Si alloy has been investigated.

2. Experimental work

Pancakes of four alloys with the nominal compositions of Nb−16% Si (A), Nb−16%Si−2%Zr (AZ2), Nb−16%Si−4%Zr(AZ4) and Nb−16%Si−6%Zr(AZ6) were prepared in a water cooled copper mould by non-consumable arc melting process under argon atmosphere using thoriated tungsten electrode. The compositions of the alloys are represented in atomic % throughout the text unless otherwise stated. The purity of raw materials used in these investigations was Nb−99.9%, Si−99.999% and Zr− 99.9%. The arc voltage of 28−32 V and arc current of 900−1000A were used during alloy preparation. The alloy pancakes were flipped over and remelted five times to achieve the chemical homogeneity. Each alloy pancake weighed about 330 grams. The phases present in the alloys were analyzed by X−ray diffraction technique using Cu−Kα (λ = 1.540562 Å) radiation. JCPDS (Joint Committee of Powder Diffraction Standards) data cards were used to identify the constituent phases. The lattice parameters of the constituent phases were measured by Cohen's method [27]. The microstructures of the alloys were investigated by scanning electron microscope (SEM) equipped with energy dispersive spectroscopy (EDS). The samples for XRD and microstructural observation and were cut from the alloy pancakes by electro discharge machining (EDM) wire cutting. The chemical compositions of the different phases present in the alloys were analyzed by a Cameca$^\Theta$ SX-100 electron probe micro−analyzer (EPMA) operating at 20 kV. The volume fractions of the phases present in the alloys were calculated using image analysis software on microstructures obtained using SEM. The orientation relationships between the phases were determined using electron backscatter diffraction (EBSD) patterns obtained in a XL30 FEG scanning electron microscope.
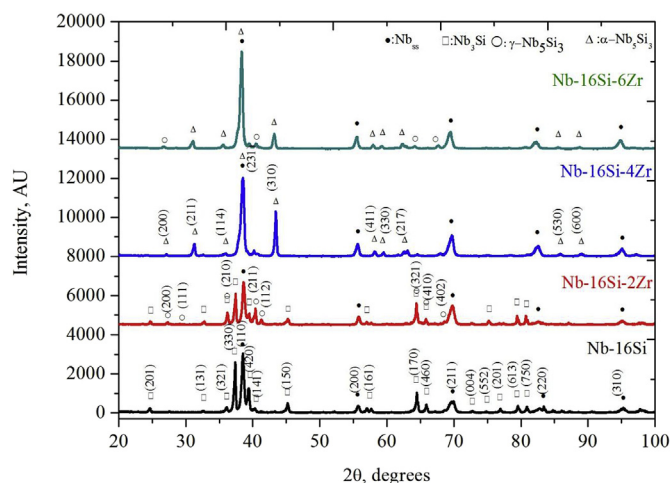

Fig. 1. X-ray diffraction patterns of Nb−16Si alloy containing different Zr levels.

3. Results

The XRD patterns of alloys studied in this work are shown in Fig. 1. It can be seen that the alloy A showed niobium solid solution (Nbss) and Nb_3Si phases whereas alloy AZ2 showed three phases consisting of Nbss, Nb_3Si and $γ−Nb_5Si_3$. The other alloy AZ4 exhibited only Nbss and $α−Nb_5Si_3$ phases while alloy AZ6 showed the existence of three phases composed of Nbss, $α−Nb_5Si_3$ and $γ−Nb_5Si_3$. The Nb_3Si phase has not been detected in alloys AZ4 and AZ6. The SEM back scattered electron micrographs of the alloys are shown in Fig. 2. It is observed that the binary alloy (A) exhibited large size (∼22–45 μm) proeutectic niobium phase in dendritic form along with eutectic mixtures consisting of Nbss and Nb_3Si phases (Fig. 2a). The alloy AZ2 also showed the two phase microstructure consisting of large size (∼15–30 μm) proeutectic niobium dendrites along with the eutectic mixtures (Nbss and Nb_3Si phases (Fig. 2b)). The fine scale eutectic mixtures composed of Nbss and $γ−Nb_5Si_3$ phases have also been noticed in some region of the microstructures. However, the volume fraction of the fine scale eutectic mixtures is very small (∼7%). In contrast, alloys AZ4 and AZ6 revealed two phase microstructures consisting of large size(∼10–28 μm) proeutectic niobium dendrites along with a mixture of Nbss and $α−Nb_5Si_3$ phases (Fig. 2c and d). The EBSD inverse pole figure (IPF) orientation image and phase mapping of alloys are depicted in Fig. 3 and Fig. 4 respectively. It can be seen that Nb phase within the domain of eutectic/eutectoid cell has same crystallographic orientations. The EBSD phase mapping results of alloys shown in Fig. 4 revealed that alloys A and AZ2 have only Nb and Nb_3Si phases whereas alloys AZ4 and AZ6 have only Nb and $α−Nb_5Si_3$ phases. The silicide phase $γ−Nb_5Si_3$ observed in interdentric region of AZ2 and AZ6 alloy has hexagonal crystal structure. A very fine secondary eutectic microstructures comprising of Nbss and $γ−Nb_5Si_3$ phases was also observed in the interdendritic regions of primary Nbss phase in AZ2 and AZ6 alloys (Fig. 4b and d).

The chemical compositions of different phases present in the alloys analyzed by EDS and EPMA are shown in Table 1. The concentration of Si in Nbss decreased from 3.2% ± 0.16 to 1.93% ± 0.08 with increasing in Zr content in the alloys. The concentration of Zr in Nbss phase was in the range from 1.16% ± 0.07 to 1.73 ± 0.08. The phase Nb_3Si in alloy AZ2 contained very small amount of Zr content (0.74 ± 0.07). The concentration of Zr in Nb_5Si_3 phase is significantly higher than that observed in Nb and Nb_3Si phases in Zr containing alloys. This shows that Zr is predominantly partitioned in Nb_5Si_3 phases rather than Nbss and Nb_3Si phase. By combining the results of SEM microstructures and EPMA, it is identified that the white colour phase corresponds to Nbss, grey contrast phase corresponds to Nb_3Si and dark
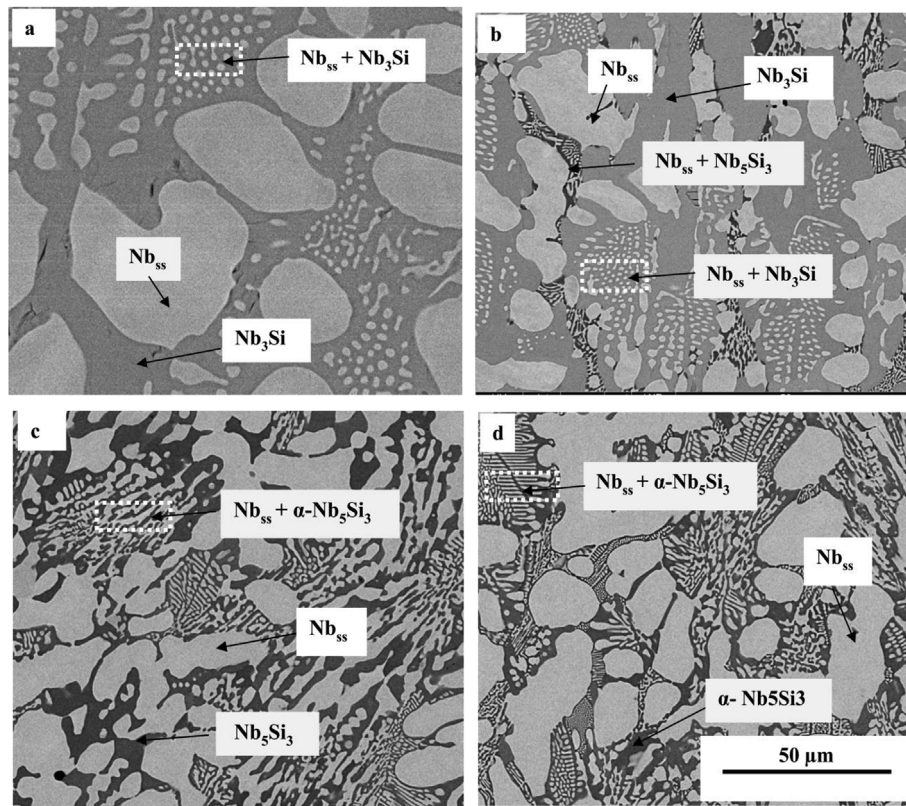
Fig. 2. SEM BSE micrographs of Nb − 16Si containing Zr: (a) 0 Zr, (b) 2Zr, (c) 4Zr and (d) 6Zr.

contrast phase corresponds to Nb_5Si_3. Table 2 shows the volume fractions of various phases present in the alloys. The volume fraction of Nb_{ss} phase and Nb_3Si phase measured in alloy A is 48.66% ± 0.61 and 51.34% ± 0.56 respectively. The volume fraction of Nb_{ss} phase is decreased from 48.66% ± 0.61 to 44.06% ± 1.59 and the volume fraction Nb_3Si phase marginally decreased from 51.34 ± 0.56 to 50.47% ± 1.63 with addition of 2%Zr (Alloy AZ2). The alloy AZ2 has an additional phase of Nb_5Si_3 with volume fraction of about 5.47% ± 0.0.07. This additional phase has been identified as hexagonal $\gamma − Nb_5Si_3$ by EBSD. The volume fraction of Nb_{ss} phase increased to 59.25% ± 0.51and 63.18% ± 1.22 with addition of 4 %Zr(AZ4) and 6 %Zr(AZ6) respectively (see Table 2). The volume fraction of Nb_5Si_3 phase in alloy AZ4 is 40.75% ± 0.54 and is decreased to 36.82% ± 0.92 in alloy AZ6. The effect of addition of Zr on the lattice parameters of various phases formed in the alloys studied in the present work as measured by Cohen's method is shown in Table 3. It can be seen from Table 3 that the lattice parameter of Nb_{ss} phase increases with increasing in the concentration of Zr. The change in lattice parameters 'a' and 'c', and c/a ratio of Nb_3Si phase in alloy A and AZ2 is also shown in Table 3. It can also be seen that the lattice parameters'a' and 'c', and c/a ratio of Nb_3Si phase in alloy A is 10.2175 Å, 5.1901 Å and 0.5079 respectively. The lattice parameter 'a' increases and 'c' decreases with addition of 2% Zr due to the substitution of Nb atom with Zr atom in Nb_3Si lattice. As a result c/a ratio of Nb_3Si phase decreases with addition of 2 %Zr. The $\alpha − Nb_5Si_3$ phase is observed only in the case of AZ4 and AZ6 alloys. The lattice parameters 'a' and 'c' of $\alpha − Nb_5Si_3$ in AZ4 alloy is 6.6366 Å and 11.7736 Å respectively. The lattice parameters 'a' of $\alpha − Nb_5Si_3$ phase decreased to 6.5932 Å while 'c' increased to 11.8718 Å with 6%Zr. Table 3 also indicate that the c/a ratio of $\alpha − Nb_5Si_3$ phase increased with increase in Zr content. The mechanism of formation of the eutectoid Nbss and $\alpha − Nb_5Si_3$ phases in Nb − Si alloys with Zr addition alloys can further be analysed using the orientation relationships between these two phases because there must be an orientation relationships between Nbss and $\alpha − Nb_5Si_3$ phases if they

are formed through eutectoid decomposition of Nb_3Si phase. Therefore, the crystallographic orientation relationships between the two phases Nbss and $\alpha − Nb_5Si_3$ were determined by EBSD. The crystallographic orientation relationship between Nb and $\alpha − Nb_5Si_3$ phases within a eutectoid lamellar colony was investigated using pole figures shown in Fig. 5. As can be seen that the orientation relationships between Nbss and $\alpha − Nb_5Si_3$ phases are (110) Nbss//(110) $\alpha − Nb_5Si_3$. The crystallographic orientation relationship obtained between primary Nbss and eutectoid $\alpha − Nb_5Si_3$ phases using pole figures is shown in Fig. 6. The orientation relationships obtained in this case are (111) Nbss//(100) $\alpha − Nb_5Si_3$.

4. Discussion

The overall composition of alloys measured by SEM EDS analysis confirmed that the composition of the alloys was close to their nominal composition.

4.1. Microstructures

SEM microstructures show (Fig. 2) that when the alloy is free of Zr (A), the microstructures consisted of Nbss and Nb_3Si phases which is in line with the finding reported by Drawin et al. [28]. However, when a small concentration of Zr is added to the alloy (AZ2), an additional phase of $\gamma − Nb_5Si_3$ had formed. The $\gamma − Nb_5Si_3$ phase is expected to form due to the enrichment of the last liquid to solidify with Zr. When the Zr concentration exceeds 2 at. %, $\alpha − Nb_5Si_3$ phase was noticed along with Nbss phase. The equilibrium microstructures consisted of Nbss and $\alpha − Nb_3Si$ phases favoured in alloys AZ4 and AZ6 in as cast condition itself.

According to Nb rich side of Nb − Si phase diagram, $\alpha − Nb_5Si_3$ phase is expected to be formed through the eutectoid decomposition of Nb_3Si phase by high temperature and long duration heat treatment. The decomposition of Nb_3Si phase in to Nbss and $\alpha − Nb_5Si_3$ phases takes
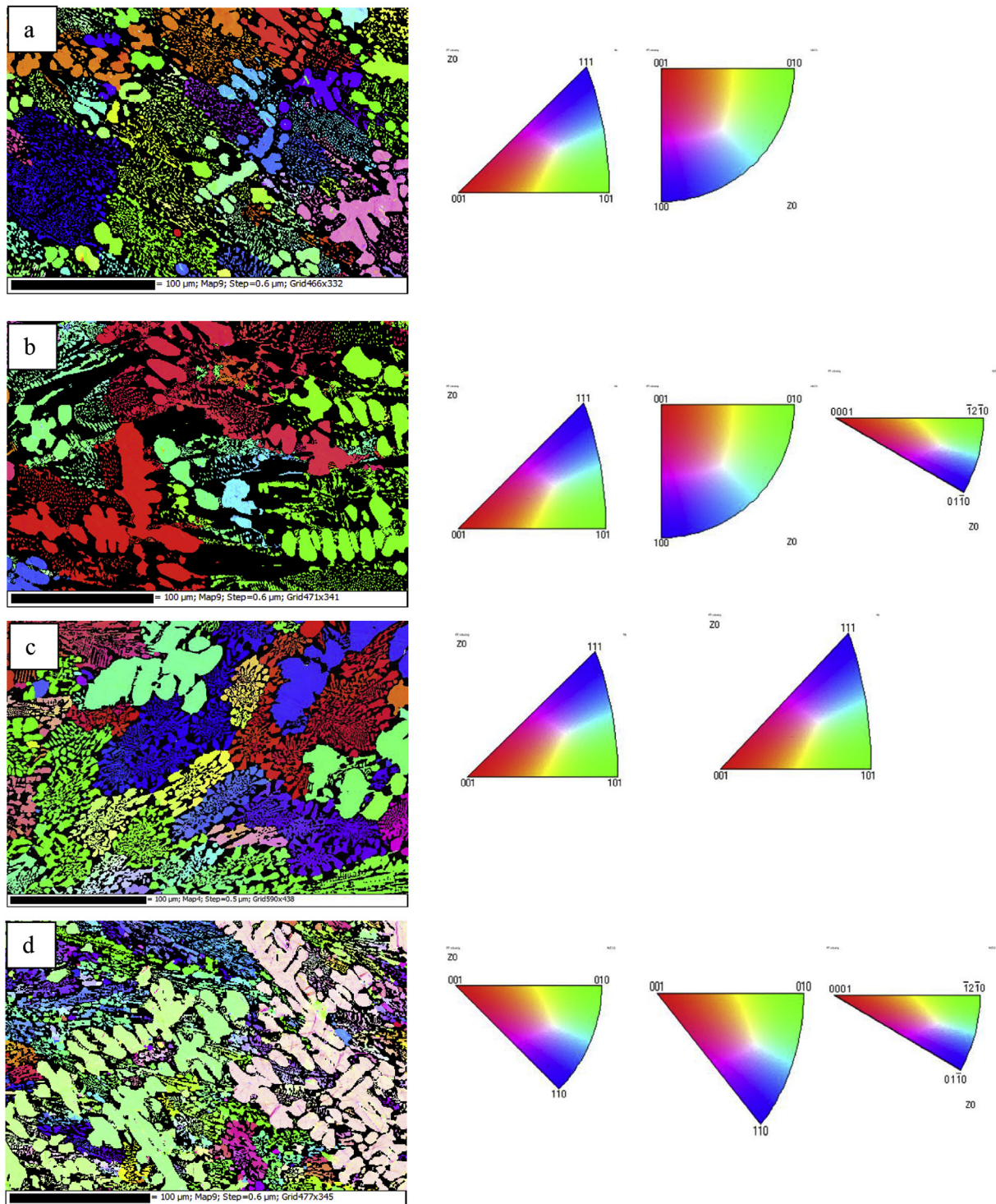
Fig. 3. EBSD IPF orientation image of $Nb-16Si$ alloy containing different Zr content: (a) 0 Zr, (b) 2Zr, (c) 4Zr and (d) 6Zr.

approximately 100 hrs to complete even at the nose of the TTT diagram (1500 °C) because of the sluggish nature of the decomposition [6–8]. Hence, there is no possibility of formation of $\alpha-Nb_5Si_3$ phase directly from the liquid phase and the high temperature phase Nb_3Si is retained at the room temperature despite the fact that $\alpha-Nb_5Si_3$ phase is the stable phase at room temperature. In the present study, as explained earlier the A and AZ2 exhibited Nb_3Si phase. The alloys AZ4 and AZ6 showed $\alpha-Nb_5Si_3$ phase in the as cast condition without any heat treatment. This is considered as a significant breakthrough as it results in considerable time and cost saving during the preparation of these

alloys. However, the mechanical properties and high temperature thermal stability of the Nbss and $\alpha-Nb_5Si_3$ phases formed in AZ4 and AZ6 alloys need to be investigated further to establish the beneficial influence of Zr additions to the $Nb-Si$ alloys.

Earlier work of addition of 1.5 at % Zr to $Nb-25Si$ alloy has been investigated by Muira et al. [24]. The $\alpha-Nb_5Si_3$ phase has not been formed in $Nb-25Si-1.5Zr$ alloy in as cast condition. However, the $\alpha-Nb_5Si_3$ phase has been reported to be formed with the subsequent heat treatment at 1400–1600 °C with duration of much shorter than that required for binary $Nb-Si$ alloys. This indicates that the kinetics of
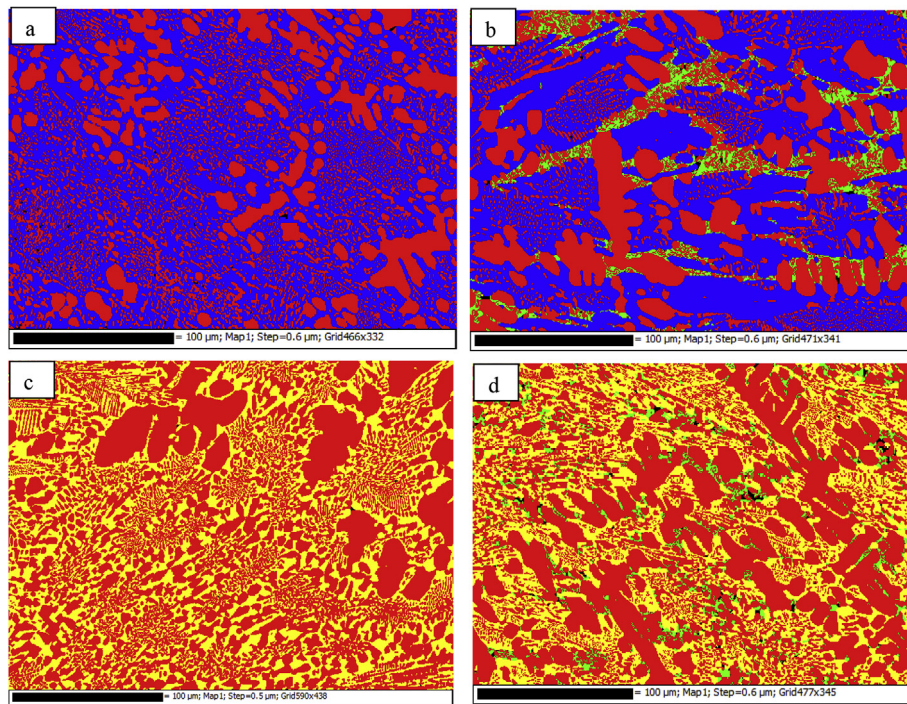
Fig. 4. EBSD phase mapping of Nb−16Si alloy containing different Zr content: (a) 0 Zr, (b) 2Zr, (c) 4Zr and (d) 6Zr.

Table 1
Compositions of the phases present in the alloys determined by EPMA.

Alloy code	Nominal alloy composition	Phases	Nb	Si	Zr
A	Nb−16Si	Nbss	96.8 ± 0.16	3.2 ± 0.16	-
		Nb₃Si	75.3 ± 0.09	24.7 ± 0.09	-
AZ2	Nb−16Si−2Zr	Nbss	95.80 ± 0.26	3.01 ± 0.21	1.19 ± 0.18
		Nb₃Si	74.87 ± 0.18	24.39 ± 0.17	0.74 ± 0.07
		Nb₅Si₃	55.88 ± 0.41	36.42 ± 0.13	7.70 ± 0.50
AZ4	Nb−16Si−4Zr	Nbss	96.45 ± 0.06	2.39 ± 0.03	1.16 ± 0.07
		Nb₅Si₃	54.93 ± 0.13	37.38 ± 0.09	7.68 ± 0.16
AZ6	Nb−16Si−6Zr	Nbss	96.34 ± 0.02	1.93 ± 0.08	1.73 ± 0.08
		Nb₅Si₃	54.94 ± 0.46	36.31 ± 0.33	8.75 ± 0.23

Table 2
Volume fraction of Nb−16Si−xZr alloys.

Nominal alloy composition (at %)	Volume fraction (%)		
	Nbss	Nb₃Si	Nb₅Si₃
Nb−16Si	48.66 ± 0.61	51.34 ± 0.56	–
Nb−16Si−2Zr	44.06 ± 1.59	50.47 ± 1.63	5.47 ± 0.07
Nb−16Si−4Zr	59.25 ± 0.51	–	40.75 ± 0.54
Nb−16Si−6Zr	63.18 ± 1.22	–	36.82 ± 0.92

eutectoid decomposition of Nb₃Si phase gets accelerated during heat treatment despite the presence of a small concentration of Zr. The possible reason for the acceleration of the kinetics of eutectoid decomposition of Nb₃Si phase may be because of reduction in interfacial energy of Nbss/Nb₅Si₃ phases with Zr [24]. However, the exact mechanism of reduction of the interfacial energy due to the presence of a small concentration of Zr is not readily available in the literature. Tian et al. [25]. reported that an alloy Nb−16%Si−24%Ti exhibited Nb and Nb₃Si phases along with fine scale eutectic mixtures composed of Nbss and γ−Nb₅Si₃ phases due to the addition of Zr(Zr = 1–4%). It indicates that addition of Zr to Nb−Si alloys in the presence of higher concentration of Ti does not form α−Nb₅Si₃ phase as Ti is a strong Nb₃Si

Table 3
Lattice parameter values of phases present in Nb−16%Si containing different concentration of Zr.

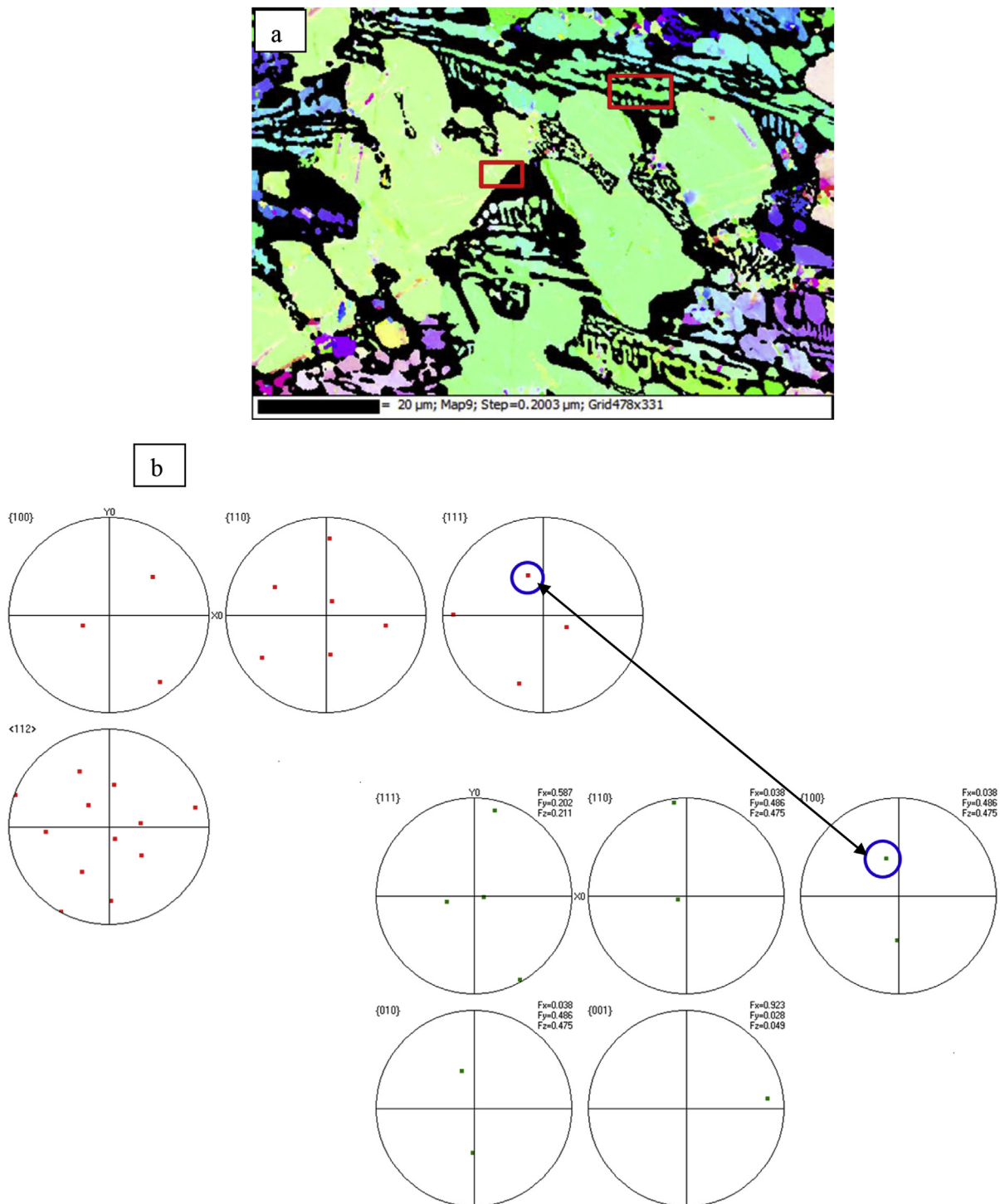| Alloy code	Lattice parameter of phases						
	Nbss a(Å)	Nb₃Si			α−Nb₅Si₃		
		a(Å)	c(Å)	c/a	a(Å)	c(Å)	c/a
A	3.2991 ± 0.0032	10.2175 ± 0.0102	5.1901 ± 0.0051	0.5079	–	–	–
AZ2	3.3021 ± 0.0033	10.2332 ± 0.0102	5.1827 ± 0.0051	0.5064	–	–	–
AZ4	3.3041 ± 0.0033	–	–	–	6.6366 ± 0.0066	11.7736 ± 0.0117	1.7740
AZ6	3.3059 ± 0.0033	–	–	–	6.6368 ± 0.0066	11.9184 ± 0.0117	1.7958

Fig. 5. (a) EBSD orientation image of Nb−16Si−6Zr alloy and (b) discrete pole figures corresponding to primary Nbss and $\alpha-Nb_5Si_3$ phase.

stabiliser.

4.2. Mechanism of phase formation

Analysis of limited number of available literature in the light of the present experimental results indicated the following two possible mechanisms.

(i) Migration of Zr to the interface between Nbss and Nb_3Si phases resulting in a reduction of the interfacial energy. This in turn, aids in the nucleation of Nbss and $\alpha-Nb_5Si_3$ phases as well as in accelerating the growth kinetics of these two phases.

(ii) Zr atoms replacing Nb atoms in the Nb_3Si lattice. Greater the quantity of Zr in the Nb_3Si lattice, greater will be the lattice distortion leading to instability of Nb_3Si phase. This enables the decomposition reaction of Nb_3Si phase to occur with ease even during solidification stage itself.

It has been reported that interfacial energy can be reduced by the microsegregation of alloying elements to the interface [29]. The segregating tendency of alloying elements is proportional to atomic size misfits. Alloying element which has large atomic size misfit tends to
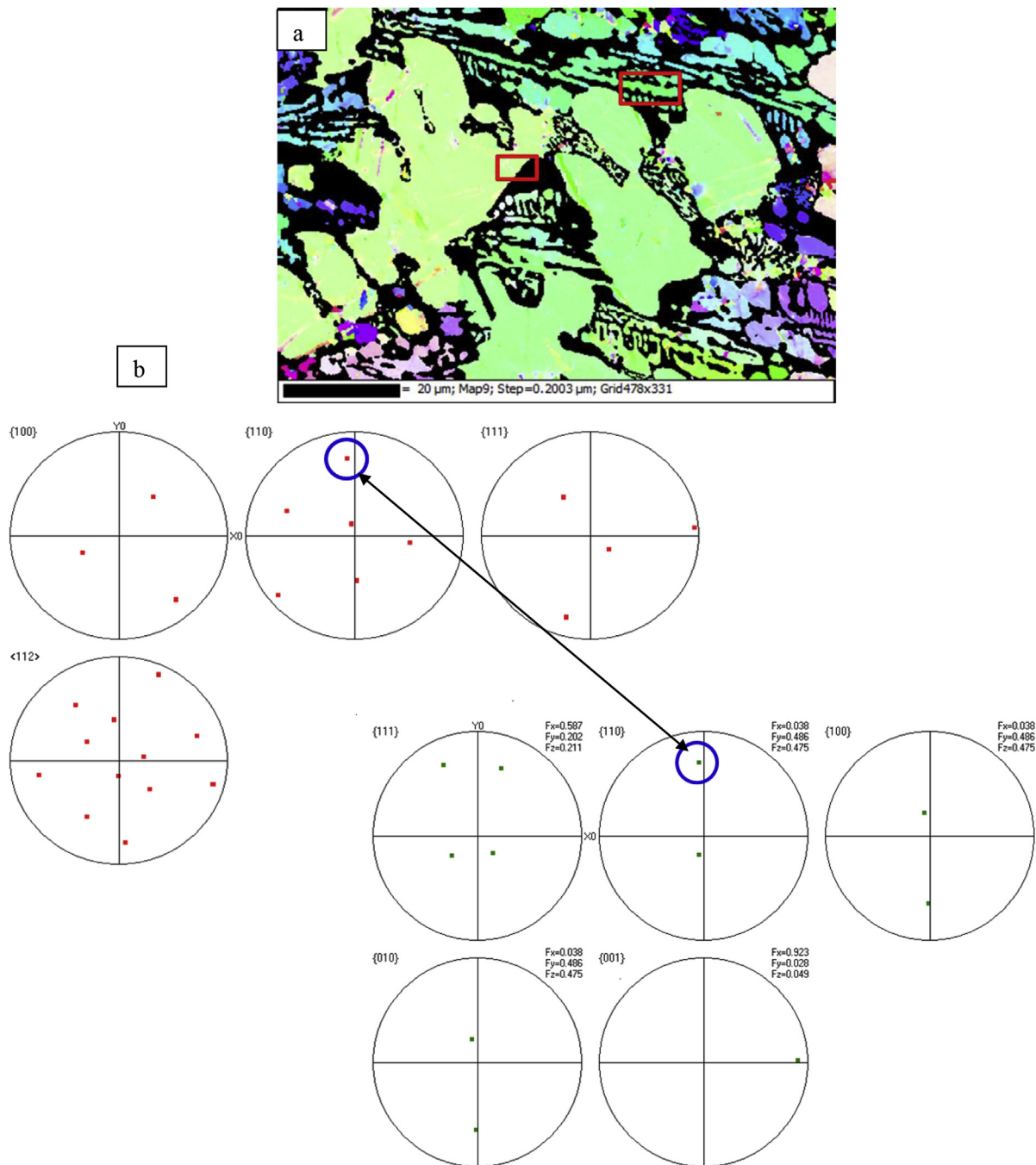
Fig. 6. (a) EBSD orientation image of Nb−16Si−6Zr alloy and (b) discrete pole figures corresponding to eutectoid Nbss and α−Nb₅Si₃ phases.

segregate more during solidification [29]. Gali et al. [30] reported that interfacial energy of the Cr−Cr₃Si eutectic composites was lowered by microalloying with Ce and Re because these elements had a tendency to segregate at the interfaces of the Cr/Cr₃Si phases. Similar kind of phenomenon may also be expected to occur in Nb−Si−Zr alloys.

Since the solubility of Zr in Nb is very limited, Zr is expected to segregate along the grain boundaries. In the present work, the preferable site for the segregation of Zr is at the interfaces between Nb and Nb₃Si phases. Thus Zr segregates at the interface reduces the interfacial energy which in turn provides more driving force for the decomposition of Nb₃Si phase during solidification. This is in agreement with the work reported by Muira et al. [24] on Nb−25Si−1.5Zr alloy where the addition of 1.5 Zr has reduced the interfacial energy. The schematic diagram showing the segregation of Zr at the interface between eutectic

Nbss and Nb₃Si phases is shown in Fig. 7. The element Zr has a BCC crystal structure at high temperature and HCP crystal structure at low temperature whereas Nb has BCC structure starting from room temperature to melting temperature. It has been reported that the eutectoid reaction in Nb−Si based alloys start by nucleation of Nb−plates at eutectic Nbss−rods/Nb₃Si matrix interface. Therefore in the present study the nucleation of eutectoid Nb plate may become easier if Zr is present at the interface of Nbss rods/Nb₃Si phases as both Zr and Nb have same crystal structure at high temperature. In the process the eutectoid Nb−plates have the same crystallographic orientation as that of Nb−rods formed by eutectic reaction. The EBSD IPZ orientation map shown in Fig. 3 clearly confirms the existence of identical orientation between eutectic Nbss rod and eutectoid Nb plates. The proposed mechanism of nucleation of Nb plates and α−Nb₅Si₃ phases through
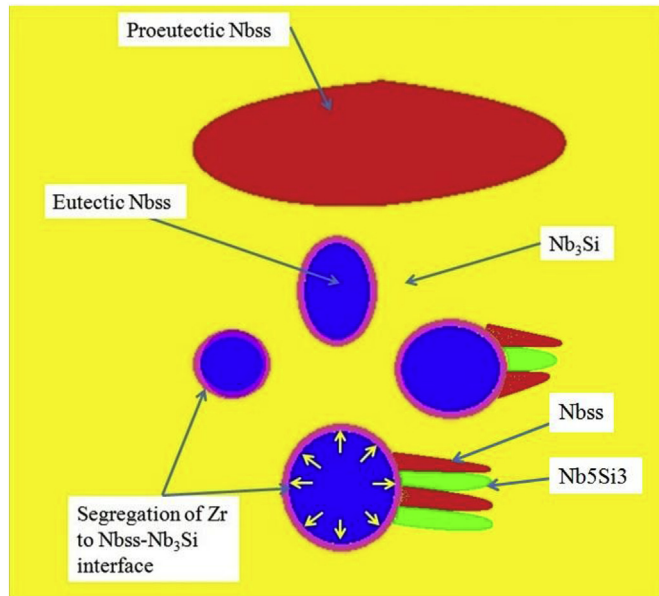
Fig. 7. Schematic diagram showing segregation of Zr and nucleation of Nb−plate at the interface between Nbss and Nb₃Si phases.

eutectoid reaction is shown Fig. 7. First Nb plates nucleate at the interface between Nb/Nb₃Si phases, then $\alpha-Nb_5Si_3$ phase nucleates when Si content at the interface of eutectoid Nb plates/Nb₃Si exceeds some critical value(~ 37.5%). There by the entire process of eutectoid transformation of Nb₃Si phase occur by the nucleation and growth of alternate layers of Nb and $\alpha-Nb_5Si_3$ phases.

The value of lattice parameter of Nbss phase increases with increase in concentration of Zr (Table 3). This can be attributed to the decrease in concentration of Si and increase in concentration of Zr in Nbss phase (Table 1). It can be understood from the lattice parameters 'a' and 'c' of Nb₃Si phase shown Table 3 that the addition of 2Zr to Nb−16Si alloy (AZ2) increased the lattice parameter 'a' and reduced the lattice parameter 'c', resulting in the reduction of c/a ratio of Nb₃Si phase. This indicates that Zr atom preferentially occupy the Nb sites in a−axes of the unit cell of Nb₃Si phase. On further increasing the concentration of Zr above 2%, the Nb₃Si phase is not observed instead $\alpha-Nb_5Si_3$ phase is noticed. It indicates that Nb₃Si phase is able to tolerate Zr concentration up to 2% in its lattice in the form of solid solution. When the Zr concentration exceeds 2%, the Nb₃Si may not be stable. Further, it is understood from the literature that even though both Nb₃Si and Zr₃Si phases belong to the same structure as Ti₃P, no solid solution is reported between Nb₃Si and Zr₃Si phases [31]. As per the phase diagram of Zr−Si, Zr₅Si₃ is a stable phase at high temperature and Zr₃Si is stable phase at low temperature. The Zr₅Si₃ phase is normally retained at low temperature during alloy preparation. The presence of interstitial impurities even at very low concentration aids the stabilisation of Zr₅Si₃ [31]. The Nb₃Si phase is not at stable when the Zr concentration is more than 2% due to the large reduction in c/a ratio resulting from the increase in lattice parameter 'a' and decrease in lattice parameter 'c'. The Nb₃Si phase is expected to decompose in to stable Nbss and $\alpha-Nb_5Si_3$

phases through eutectoid transformation during solidification to reduce the lattice strain/distortion. As a result, the alloys with 4Zr and 6Zr concentration yielded the equilibrium microstructures composed of Nbss and $\alpha-Nb_5Si_3$ phases in the as cast condition.

The identification of orientation relationships between the phases plays a significant role in order to understand phase formation during solid state phase transformation. The orientation relationships measured between Nbss and $\alpha-Nb_5S_3$ phases and those reported by the different authors on Nb−Si based alloys are shown in Table 4. It should be noted that the orientation relationships obtained for Nbss and $\alpha-Nb_5Si_3$ phases ((110) Nbss//(110) $\alpha-Nb_5Si_3$)) in this study are same as that of the orientation relationships obtained for Nbss and $\alpha-Nb_5Si_3$ phases in Nb−16Si and Nb−22Si alloys by Drawin et al. [28] and in Nb−25Si−1.5Zr alloy by Muira et al. [24] respectively after the heat treatment. Hence, It is confirmed that in the present work the formation of Nbss and $\alpha-Nb_5Si_3$ phases in alloys AZ4 and AZ6 is mainly due to the eutectoid decomposition of Nb₃Si phase(Nb₃Si → Nbss + $\alpha-Nb5Si3$) which occurs in the process of solidification of alloys itself.

4.3. Morphology of the phases

It is well known that the morphology of phases formed in an eutectic alloy is decided by nature of the interface. In some cases the volume fraction of the constituent phases also plays a role in selection of a particular morphology. Jackson derived a parameter which is defined as $\alpha = \Delta S_f/R$, where ΔS_f is the entropy of fusion and R is the gas constant [32]. If the value of α is less than 2 the phase tends to have a non−faceted interfaces, while if the value of α is greater that than 2 the other interfaces are likely to occur. Thus the entropy of fusion of constituent phases is the deciding factor in the formation of different types of interfaces. Further, the eutectic microstructure can be of regular or irregular morphology depending on the weather the interface is grown in facetted or non-facetted manner. Usually the metallic system has a non−faceted interface as it has low entropy of fusion while covalent and ionic bonded materials have a faceted interface as its entropy of fusion is very high. In Nb−Si alloy system, Nbss phase has a non−-faceted interface with liquid ($\Delta S_f = 9.6 \, J \, mol^{-1} \, K^{-1}$, $\alpha = 1.2$) while the silicides, Nb₃Si/Nb₅Si₃ have a faceted interface with liquid ($\Delta S_f = 64.6 \, J \, mol^{-1} \, K^{-1}$, $\alpha = 2.4$) [33]. Therefore, the eutectic phases are expected to be grown in a divorced manner (i.e. uncooperative growth). As a result the microstructure of Nb−Si alloys will have an irregular morphology.

The alloys A and AZ2 have shown the presence of Nbss in two different forms. One is the proeutectic Nbss with dendritic morphology while the other one exhibited of rod morphology (Fig. 2a and b) in a continuous matrix of Nb₃Si phase. In contrast, the alloys AZ4 and AZ6 exhibited proeutectic Nbss with dendritic morphology together with eutectoid Nbss in plate morphology. The microstructure of these alloys revealed the presence of $\alpha-Nb_5Si_3$ phase. The eutectoid microstructures (Nbss and $\alpha-Nb_5Si_3$) have regular lamellar morphologies (Fig. 2c and Fig. 2d) as against the irregular morphologies of eutectic microstructures (Fig. 2a and 2b). The interlamellar spacing (λ) of Nbss and $\alpha-Nb_5Si_3$ phases can be defined as the distance from the center of the Nbss lamellae to the center of the $\alpha-Nb_5Si_3$ lamellae. It may be

Table 4
Orientation relationships between Nb and $\alpha-Nb_5Si_3$ phases in Nb−Si alloys.

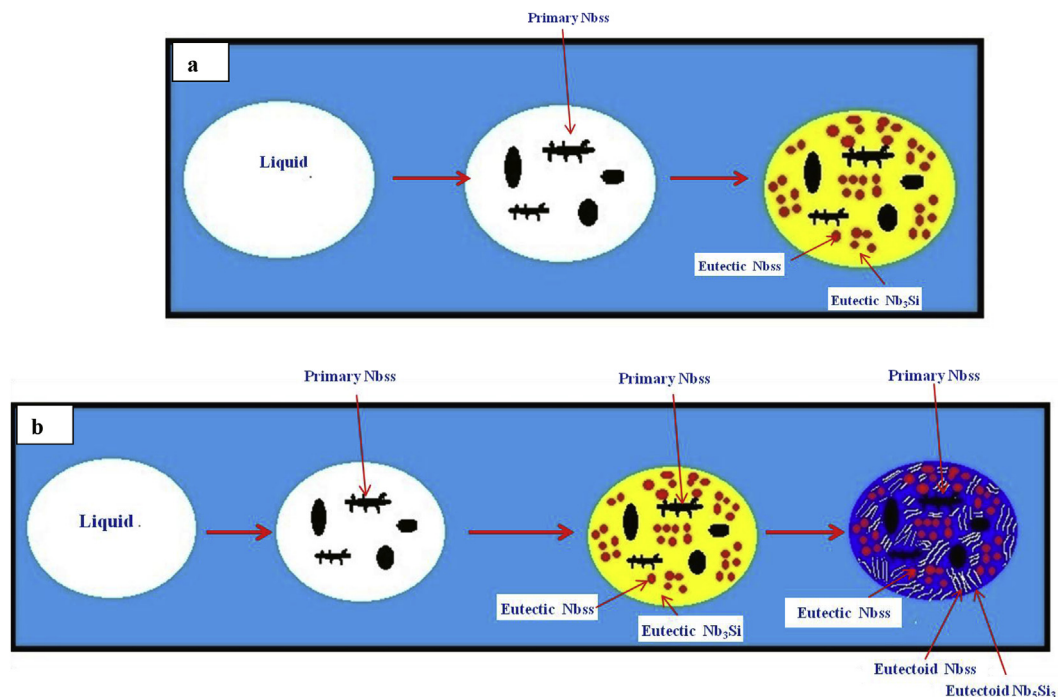| Alloys (at. %)	Method of alloy preparation & heat treatment	Characterisation tools used	Orientation relationship	References
Nb-16Si Nb-22Si	Non-consumable arc melting HT@1500 °C for 75 h	EBSD	(011)$\alpha-Nb_5Si_3$//(011)Nb (100) $\alpha-Nb_5Si_3$//(111)Nb	S.Drawin et al. [28]
Nb−25Si Nb−25Si−1.5Zr	Arc melting HT@1100 °C to1650 °C for 3 to 100 h	EBSD	Binary alloy (001)Nb₅Si₃//(001)Nb Ternary alloy ((110)Nb₅Si₃//(011)Nb	S.Muira et al. [24]
Nb−16Si−4Zr	Non-consumable arc melting	EBSD	(011)$\alpha-Nb_5Si_3$//(011)Nb (100) $\alpha-Nb_5Si_3$//(111)Nb	The present work

Fig. 8. Solidification sequence of (a) $Nb-16Si$ and $Nb-16Si-2Zr$, and (b) $Nb-16Si-(4–6)$ Zr alloys.

noted that the interlamellar spacing between Nbss and $\alpha-Nb_5Si_3$ phases coarse in the case of alloy AZ4 as compared to alloyAZ6 in which the Zr concentration is higher. This suggests that presence of Zr strong influence on both nucleation and growth of the Nb/Nb_5Si_3 lamellar structure. The size of the interlamellar spacing mainly depends on the velocity of the interface growth. It is generally inversely proportional to the growth rate. Therefore, in the present study, it may be inferred that the larger interlamellar spacing noticed in AZ4 alloy is related to slower growth rate while smaller interlamellar spacing observed in AZ6 alloy is related to faster growth rate. The faster growth rate in alloy AZ6 in turn confirm that the presence of higher Zr concentration in $Nb-Si$ alloys increases/accelerates the kinetic of eutectoid decomposition of Nb_3Si phase during solidification.

Based on the results of SEM BSE micrographs, EPMA analysis and EBSD images, a possible solidification sequence of the alloys is proposed as depicted in Fig. 8. The solidification paths of the A and AZ2 alloys are same (Fig. 8a) except for some fine scale secondary eutectic microstructure comprising of Nbss and $\gamma-Nb_5Si_3$ phases observed at the interdendritic region of proeutectic Nb phase due to segregation of Zr. The solidification sequence of AZ4 and AZ6 alloys are same (Fig. 8b). However, the EBSD phase mapping (Fig. 4d) revealed that the alloy AZ6 also exhibited fine scale secondary eutectic microstructure comprising of Nb and $\gamma-Nb_5Si_3$ phases similar to the one observed in AZ2 alloy.

5. Conclusions

The microstructure and phase formation of $Nb-16Si$ alloy containing different Zr concentrations was systematically investigated. The following conclusions are drawn.

1. The alloys $Nb-16Si$ (A) and $Nb-16Si-2Zr$(AZ2) exhibit similar kind of microstructures consisting of Nbss and Nb_3Si phases. The alloys $Nb-16Si-4Zr$ (AZ4) and $Nb-16Si-6Zr$ (AZ6) reveal two phase microstructures composed of Nbss and $\alpha-Nb_5Si_3$ phases. The minor fraction of $\gamma-Nb_5Si_3$ phase is observed in alloys AZ2 and AZ6 in the interdendritic region.
2. The equilibrium microstructures consist of Nbss and $\alpha-Nb_5Si_3$

phases are obtained in alloys AZ4 and AZ6 in the as cast condition itself without any high temperature heat treatment. The addition of Zr accelerates the dissociation kinetics of Nb_3Si phase in to Nbss and $\alpha-Nb_5Si_3$ phases during solidification. This eliminates heat treatment required for decomposition of Nb_3Si phase in Nb-Si alloys.
3. The lattice parameter of niobium solid solution (Nbss) phase increases with increase in concentration of Zr. The lattice parameter of Nb_3Si phase 'a' expands and 'c' contracts in alloy AZ2 as compared to alloy A. The lattice parameter of $\alpha-Nb_5Si_3$ phase 'a' decreases and 'c' increases with increase in Zr concentration.
4. The segregation of Zr at the interface between Nbss and Nb_3Si phases and instability of Nb_3Si phase with increase in Zr concentration of above 2 at. % Zr is responsible for formation of Nbss and $\alpha-Nb_5Si_3$ phases in the as cast condition. The alloying element Zr is predominantly partitioned in Nb_5Si_3 phases.
5. The Lamellar microstructure consisting of Nb_{ss} and $\alpha-Nb_5Si_3$ phase is obtained in alloy AZ4 and AZ6. The orientation relationship between eutectoid lamellar Nb_{ss} and $\alpha-Nb_5Si_3$ phases is determined as (110) $Nb//(110)$ Nb_5Si_3.

Acknowledgement

References

[1] B.P. Bewley, M.R. Jackson, J.C. Zhao, Ultrahigh-temperature $Nb-$silicide based composites, MRS Bull. 28 (9) (2003) 636–646.
[2] B.P. Bewlay, M.R. Jackson, J.C. Zhao, P.R. Subramanian, A review of very high temperature Nb silicide$-$based composites, Metall. Mater. Trans. A 34 (10) (2003) 2043–2052.
[3] P.R. Subramanian, M.G. Mendiratta, D.M. Dimiduk, M.A. Stucke, Advanced intermetallic alloys$-$beyond gamma titanium aluminides, Mater. Sci. Eng., A $239-240$

(1997) 1–13.

[4] N. Sekido, Y. Kimura, S. Miura, F.G. Wei, Y. Mishima, Fracture toughness and high temperature strength of unidirectionally solidified Nb−Si binary and Nb−Ti−Si ternary alloys, J. Alloys compd. 425 (2006) 223–229.

[5] P.R. Subramanian, M.G. Mendiratta, D.M. Dimiduk, Microstructures and mechanical behavior of Nb-Ti base beta + silicide alloy, Mater. Res. Soc. Symp. Proc. 322 (1994) 491–502.

[6] S. Chan, Modelling creep behaviour of niobium silicide in-situ composites, Mater. Sci. Eng., A 337 (2002) 59–66.

[7] B.P. Bewley, S.D. Sitzman, L.N. Brewer, M.R. Jackson, Analyses of eutectoid phase transformation in Nb−Silicide in situ composites, Microsc. Microanal. 10 (2004) 470–480.

[8] M.G. Mendiratta, D.M. Dimiduk, Phase relations and transformation kinetics in the high Nb region of the Nb−Si system, Scripta Metall. 25 (1) (1991) 237–242.

[9] M.E. Schlesinger, H. Okamoto, A.B. Gokhale, R. Abbaschian, The Nb-Si (Niobium-Silicon), system, J. Phase Equil. 14 (1993) 502–509.

[10] Y. Sainan, J. Lina, S. Linfen, M. Limin, Z. Hu, The microstructure evolution of directionally solidified Nb-22Ti-14Si-4Cr-2Al-2Hf alloy during heat treatment, Intermetallics 38 (2013) 102–106.

[11] S. Zhang, X. Guo, Alloying effects on the microstructure and properties of Nb−Si based ultrahigh temperature alloys, Intermetallics 70 (2016) 33–44.

[12] D. Yonghua, Stability, elastic constants and thermodynamic properties of (α. B, γ) Nb₅Si₃ phases, Rare Metal Mater. Eng. 44 (1) (2015) 18–23.

[13] L. Zifu, P. Tsakiropoulos, Study of the effects of Ge addition on the microstructure Nb−18Si in situ composites, Intermetallics 18 (2010) 1072–1078.

[14] M. Wu, Y. Wang, S. Li, L. Jiang, Y. Han, Effect of Si on microstructure and fracture toughness of directionally solidified Nb Silicide alloys, Int. J. Mod. Phys. B 24 (15−16) (2010) 2964–2969.

[15] B.P. Bewley, M.R. Jackson, H.A. Lipsitt, The balance of mechanical properties and environmental properties of a multielement niobium−niobium silicide based in situ composite, Metall. Mater. Trans. A 27 (1996) 3801–3808.

[16] M.R. Jackson, B.P. Bewlay, R.G. Rowe, D.W. Skelly, H.A. Lipsitt, High-temperature refractory metal-intermetallic composites, JOM 48 (1996) 39–44.

[17] D.L. Davidson, K.S. Chan, The Fatigue and fracture resistance of a Nb−Cr−Ti−Al Alloy, Metall. Mater. Trans. A 30 (1999) 2007–2018.

[18] J. Geng, P. Tsakiropoulos, G. Shao, Oxidation of Nb−Si−Cr−Al in situ composites with Mo, Ti and Hf additions, Mater. Sci. Eng., A 441 (2006) 26–38.

[19] H. Liang, Y.A. Chang, Thermodynamic modeling of the Nb−Si−Ti ternary system, Intermetallics 7 (1999) 561–570.

[20] Y. Yang, Y.A. Chang, J.C. Zhao, B.P. Bewley, Thermodynamic modeling of the Nb–Hf–Si ternary system, Intermetallics 11 (2003) 407–415.

[21] W.Y. Kim, H. Tanaka, A. Kasama, S. Hanada, Microstructure and room temperature fracture toughness of Nbₛₛ/Nb₅Si₃ in situ composites, Intermetallics 9 (2001) 827–834.

[22] S. Kashyap, C.S. Tiwary, K. Chattopadhyay, Effect of Gallium on microstructure and mechanical properties of Nb−Si eutectic alloy, Intermetallics 19 (2011) 1943–1952.

[23] B. Paira, T. Kansabanik, K. Biswas, R. Tewari, Effect of chromium on microstructure and mechanical properties of Nb-Si hypoeutectic and eutectic alloys, Trans. Indian Inst. Met. 68 (6) (2015) 1039–1046.

[24] S. Miura, Y. Aoki, K. Ohkubo, T. Mohri, Y. Mishima, Effects of Zr on the eutectoid decomposition behaviour of Nb₃Si into (Nb)/Nb₅Si₃, Metall. Mater. Trans. 36 (2005) 489–496.

[25] X. Tian, J.T. Guo, L.Y. Sheng, G.M. Cheng, L.Z. Zhou, L.L. He, H.Q. Ye, Microstructure and mechanical properties of cast Nb-Ti-Si-Zr alloys, Intermetallics 16 (2008) 807–812.

[26] B.P. Bewlay, C.L. Briant, A.W. Davis, M.R. Jackson, The effect of silicide volume fraction on the creep behaviour of Nb-silicide based in-situ composites, Mater. Res. Soc. Symp. Proc. 646 (2001) 271–276.

[27] B.D. Cullity, Elements of X-ray Diffraction, second ed., Addison−Wesley Publishing Company INC, Reading, MA, USA, 1978, pp. 363–367.

[28] S. Drawin, P. Fetit, D. Boivin, Microstructural properties of Nb-Si alloys investigated using EBSD at large and small scale, Metall. Mater. Trans. 36 (2005) 497–505.

[29] H. Bei, G.M. Pharr, E.P. George, A review of directionally solidified intermetallics composites for high temperature structural applications, J. Mater. Sci. 39 (12) (2004) 3975–3984.

[30] A. Gali, H. Bei, E.P. George, Thermal stability of Cr−Cr₃Si eutectic microstructures, Acta Mater. 57 (13) (2009) 3823–3829.

[31] L. Brewer, O. Krikorian, Reaction of refractory silicides with carbon and nitrogen, J. Electrochem. Soc. 103 (1956) 38–51.

[32] D.P. Woodruff, The Solid−liquid Interface, Cambridge University Press, London, 1973, pp. 40–43.

[33] Y. Li, S. Miura, K. Ohsasa, C. Ma, H. Zhang, Ultrahigh-temperature Nbss/Nb₅Si₃ fully Lamellar microstructure developed by directional solidification in OFZ furnace, Intermetallics 19 (2011) 460–469.